Materials Chemistry and Physics 295 (2023) 126986

Contents lists available at ScienceDirect

Materials Chemistry and Physics

journal homepage: www.elsevier.com/locate/matchemphys

Dielectric properties of graphene/nano-Fe_2O_3 filled poly (vinyl alcohol)/ Chitosan blends

Priyanka Rani [a], Kalim Deshmukh [b], Jaroslav Kadlec [b], T.V. Krishna Karthik [c], S.K. Khadheer Pasha [a,*]

[a] Functional Nanomaterials and Nanocomposite Laboratory, Department of Physics, VIT-AP University, Amaravati, Guntur, 522237, Andhra Pradesh, India
[b] New Technologies - Research Center, University of West Bohemia, Plzeň, Czech Republic
[c] Autonomous Hidalgo State University, Tepeji Graduate School, Industrial Engineering, Mexico

HIGHLIGHTS

- GQDs and Fe_2O_3 NPs reinforced PVA/CS blend nanocomposites were prepared.
- High dielectric constant and low loss tangent were observed for nanocomposites.
- Nanocomposites were characterized using FTIR, XRD, SEM and TGA.
- Cole-cole plot and equivalent circuits were obtained from impedance data.

GRAPHICAL ABSTRACT

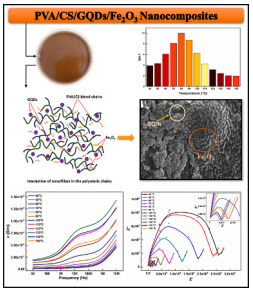

ARTICLE INFO

Keywords:
Impedance
GQDs
Fe_2O_3
Dielectric properties
Chitosan
Cole-cole

ABSTRACT

Novel nanocomposites based on Poly (vinyl alcohol) (PVA), Chitosan (CS), Graphene quantum dots (GQDs) and iron oxide (Fe_2O_3) nanoparticles (NPs) have been synthesized by solution casting method. The structural modifications and morphological studies were carried out by Fourier transform infrared (FTIR) spectroscopy, X-ray diffraction (XRD) and Scanning electron microscopy/Energy-dispersive X-ray (SEM/EDX) techniques. The results confirm the microscopic interactions and sphere-like morphology of the nanocomposites due to the presence of GQDs and Fe_2O_3 within the polymer blend. The thermal stability with almost 25% leftover residue for higher nanofillers loading in the nanocomposite was estimated by thermo-gravimetric analysis (TGA). Moreover, the frequency and temperature-dependent dielectric properties were investigated. The dielectric constant and loss tangent values are greatly influenced by reinforcement of GQDs/Fe_2O_3 and the obtained values were in the range of $\sim 10^4$ and $\sim 10^1$, respectively at 150 °C and 50 Hz. The rise in ac conductivity i.e., 9.8 x 10^{-4} (S/m) with increasing nanofiller loadings suggests the reduction in capacitive reactance and impedance. However, the semi-circular arcs are observed in the cole-cole plot where the fitted impedance data along with the equivalent circuit is also presented. The reduction of bulk resistance and impedance on increasing the nanofiller loadings with enhanced dielectric properties signifies the use of PVA/CS/GQDs/Fe_2O_3 nanocomposites as a potential material for energy storage applications.

* Corresponding author.
E-mail address: khadheerbasha@gmail.com (S.K. Khadheer Pasha).

https://doi.org/10.1016/j.matchemphys.2022.126986
Received 15 August 2022; Received in revised form 21 October 2022; Accepted 1 November 2022
Available online 4 November 2022

1. Introduction

Nanocomposites (NCs) having at least 1 nanometre (nm) dimension have potential applications due to their high-level performance, design possibilities and combination of exceptional properties. NCs consisting of matrix and reinforcement phase provides improved properties depending upon the reinforced nano-filler [1]. NCs are classified into three different categories on the basis of added nanofiller and the high quantity matrix material used [2]. They are metal nanocomposites (MNCs) [3], ceramic nanocomposites (CNCs) [4], and polymer nanocomposites (PNCs) [5]. Among them, PNCs have shown tremendous potential in various technological applications [6,7]. PNCs are nanoscale materials that have a wide variety of applications and are manufactured by blending inorganic particles having varying properties with an organic polymer matrix. PNCs are polymer matrices that have been implanted with nanoscopic components and acquire good flexibility and processability [8]. Typically, polymers are comprised of monomers that have flexible, lightweight, and low-cost manufacturing features. On mixing it with inorganic nanoparticles (NPs) having excellent electrical, mechanical, catalytic, and magnetic properties, a new material with a wide variety of applications can be produced [9,10]. Because of their superior mechanical, dielectric, optical, thermal, electrical, barrier, and other physical and chemical properties, PNCs are a viable alternative to traditional composites. The high surface-to-volume ratio of these materials allows them to drastically alter the inherent characteristics of a polymer matrix at extremely low nanofiller content [11]. In addition, PNCs offer excellent gas and water vapour barrier characteristics where the kind of nanofiller, their aspect ratio, and NCs structure all have a role to play in reducing gas permeability [12]. In general, PNCs containing completely exfoliated NPs with high aspect ratios would have the best gas barrier capabilities. In the last few decades, PNCs have been extensively studied and due to their fascinating dielectric characteristics, PNCs have potential uses in flexible electronics [13]. Despite the polymer matrix, nanofillers are considered to be very important for preparation of NCs. Various nanomaterials such as, metal oxides [14], semiconductors [15], carbon black [16], fullerenes [17], nanotubes [18], graphene-based materials [19], etc., can be reinforced within polymer matrix [20]. Additionally, NPs own higher surface area as compared to their microscale counterparts, which supports the filler-matrix interactions and as result improves the performance of the resulting materials. The PNCs with high dielectric strength and high energy density have shown considerable potential in electrical energy storage applications [21]. Generally, polymers possess high breakdown strength but low dielectric strength, while NPs show high dielectric strength but are fragile and unable to withstand large electric fields. So, for enhancing the dielectric strength of polymers, the nanofillers with high dielectric constant can be incorporated. Though, a significant concentration of nanofillers is required to effectively strengthen the dielectric constant of PNCs, which may produce filler agglomeration and add unavoidable pores and other defects to the composites [22]. Thus, PNCs have garnered considerable interest for their wide range of applications in various sectors including automotive, electronics, packaging, engineering, and aviation fields [23,24].

Furthermore, in the area of renewable energy sources, there is an increasing demand for efficient electrical energy storage devices. Dielectric capacitors provide a higher operating voltage and power density, a longer life span, and better cycle stability than batteries and electrochemical capacitors [25]. Apart from this, high-k dielectric materials have gained tremendous attention. Nanofillers in the polymer matrix with homogeneous dispersion have an essential effect on improving certain functional properties of the PNCs. Poly (vinyl alcohol) (PVA) is hydrophilic in nature, a non-toxic and synthetic-type of polymer that allows nanofillers to disperse well. It's a promising material with great chemical resistance, dielectric and tensile strength, charge storage capacity, and dopant-dependent optical and electrical characteristics [26]. PVA is employed in coating materials, functional membranes, drug delivery, fuel cells, and biomaterial applications because it generates films that are transparent and show good improvement in physical and chemical properties [27,28]. Chitosan (CS), a nontoxic and natural biopolymer. CS is a biodegradable polymer with extremely excellent film-forming properties [29]. When PVA and CS are combined together, they demonstrate better mechanical and chemical properties due to the specific intermolecular interactions between their chains. Many researchers in the fields of membrane filtration, biomedicine, packaging and dye adsorption have explored the combined impact of these two polymers [30,31]. Also, exfoliated graphite nanoplatelets, graphene quantum dots (GQDs) and carbon nanofillers have a higher dielectric constant, high carrier mobility, a large specific surface area and good thermal as well as electrical conductivity [32]. Graphene and its functionalized forms like graphene nanoribbons or reduced graphene oxide are frequently recommended as useful dielectric materials due to their ability to improve the electrical conductivity, dielectric characteristics, and mechanical robustness of polymeric materials [33]. Because of their facile aggregation and poor dispersion in several common solvents, 2D graphene sheets are only partially suitable [34]. Graphene nanoribbons, on the other hand, minimize these issues while validating the intriguing traits of limited transport gaps and quantum dot behaviour. GQDs, which are nm sized zero-dimensional materials have received a lot of attention as they exhibit the outstanding features of graphene and the edge effect of quantum dots [35]. GQDs offer remarkable qualities such as minimal toxicity and high biocompatibility. In addition, GQDs have a high solubility in a range of solvents, unlike graphene, which tends to agglomerate and disperse poorly. GQDs offer great features such as a large surface area, efficient electron transport, and bright luminescence. Several research groups have focused on increasing the dielectric constant of PVA and CS matrix-based PNCs by using a variety of inorganic and organic fillers like $BaTiO_3$, CuO, graphite, and SiC, among others [36,37]. However, to develop a nanocomposite with a high dielectric constant, most of these fillers are employed in large quantities. In the nanocomposite, this results in poor mechanical performance, limited flexibility, toxicity, brittleness, and low breakdown strength. When a large quantity of heat is created during operation, high dielectric constant and good electrical conductivity are crucial material qualities. Flexible dielectric material with high electrical conductivity, dielectric constant, and comparatively low dielectric loss is highly desirable for increasing the lifespan of PNCs through heat dissipation, which is necessary for the energy industry [38].

Iron (III) oxide (Fe_2O_3) NPs have a wide variety of applications and are intensively studied both in organic as well as inorganic matrices. These materials have unique electrical, magnetic, optical, and biological characteristics that cannot be found in bulk materials [39,40]. These ferromagnetic NPs may be distributed into appropriate solvents, generating homogenous suspensions known as ferrofluids, with correct surface coating. Fe_2O_3 NPs dispersion characteristics and their compatibility with various organic solvents regulate their real use in different practical applications [41]. Since, Fe_2O_3 NPs are easily available and less expensive than other nanoscale fillers, they might be a good choice for practical applications. They also have multi-functional capabilities. The nanocrystalline Fe_2O_3 has potential uses in solar energy conversion, optical, and magnetic films, etc. In recent years, γ-Fe_2O_3 has been extensively employed as a form of gas-sensing material for the detection of flammable gases, harmful pollutant gases and organic vapours [42,43]. In this work, GQDs and Fe_2O_3 are dispersed in PVA/CS blend and the prepared PVA/CS/GQDs/Fe_2O_3 nanocomposites are examined for the investigation of their morphological, thermal, electrical and dielectric properties.

Table 1
Feed composition for PVA/CS/GQDs/Fe_2O_3 nanocomposite having different GQDs and Fe_2O_3 loadings.

Sr. No	PVA (wt %)	Chitosan (wt %)	Iron Oxide NPs (wt%)	Graphene Quantum dots (GQDs) (wt%)
1	100	0	0	0
2	50	50	0	0
3	50	39	10	1
4	50	28	20	2
5	50	17	30	3

2. Experimental section

2.1. Materials

CS powder was supplied by Sisco Research Laboratories Pvt. Ltd., India. Poly (vinyl alcohol) (PVA) powder with 1,15,000 molecular weight was procured from Loba Chemie Pvt. Ltd. Mumbai, India. Graphene quantum dots (GQDs) (1 mg/ml) of M.W. 12.01 and glacial acetic acid of ≥99.7% purity was procured from Sigma-Aldrich (Merck) Pvt. Ltd., India. Iron (III) oxide (Fe_2O_3) nanopowder of <50 nm particle size was procured from Sisco Research Laboratories Pvt. Ltd., India.

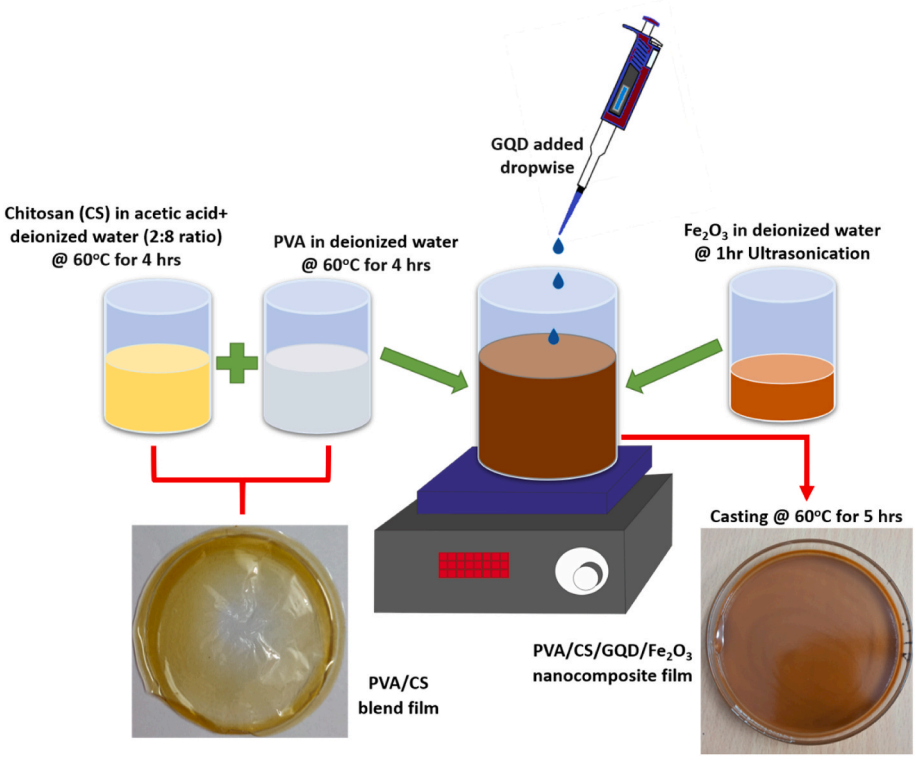

Fig. 1. Schematic procedure of PVA/CS blend film and PVA/CS/GQDs/Fe_2O_3 nanocomposite film preparation via solution casting method.

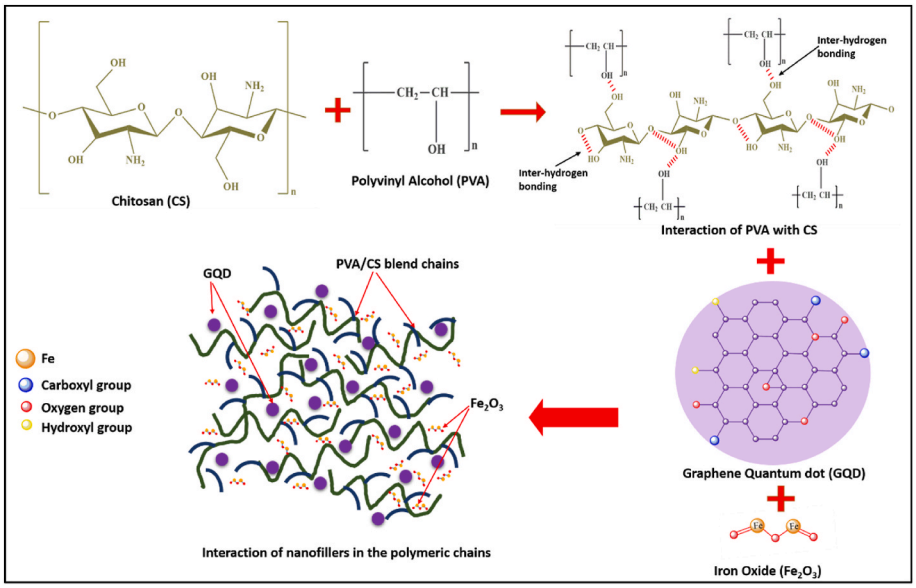

Fig. 2. Schematic diagram of possible chemical interaction of GQDs and Fe_2O_3 within the polymeric chains of PVA/CS blend.

2.2. Preparation of PVA/CS/GQDs/Fe_2O_3 nanocomposite film

2.2.1. Synthesis of PVA/CS blend

To begin with, 0.5 g of PVA powder was dissolved in 20 ml deionized water via heating at 60 °C for 4 h followed by stirring to obtain transparent solution. Simultaneously, 0.5 g of CS powder was dissolved in a mixed solution of acetic acid: deionized water (2:8) by heating and stirring at 60 °C for 4 h. Later on, both the solutions are added together via stirring at room temperature (RT) for 8 h. The obtained homogenous solution is further transferred into a clean glass petri dish for casting at 60 °C for 3 h. The smooth and flexible PVA/CS blend film was peeled off and preserved at room temperature for further characterizations.

2.2.2. Synthesis of PVA/CS/GQDs/Fe_2O_3 nanocomposite film

The PVA/CS/GQDs/Fe_2O_3 nanocomposite films with various loadings of GQDs and nano-Fe_2O_3 as mentioned in Table 1 are prepared by a simple solution casting approach. The earlier prepared PVA/CS blend solution is used for nanocomposite preparation. GQDs of the desired amount is added dropwise in the polymer blend solution and stirred for homogenous mixing. Further, the Fe_2O_3 solution prepared by dispersing Fe_2O_3 nanopowder in 10 ml deionized water through ultrasonication at RT for 1 h followed by vigorous stirring is added in PVA/CS/GQDs solution. The PVA/CS/GQDs/Fe_2O_3 solution was further stirred for nearly ~12 h in order to obtain the homogenous dispersion. At last, the uniformly dispersed solution was collected in the glass petri dish for casting at 60 °C temperature for 5 h. Fig. 1 provides the systematic preparation of PVA/CS/GQDs/Fe_2O_3 nanocomposite film. Additionally, the chemical interaction occurring between the PVA and CS along with the possible interaction of GQDs and Fe_2O_3 within the polymer blend is demonstrated in Fig. 2.

3. Characterization details

Fourier transform infrared (FTIR) spectra of neat PVA, PVC/CS blend, and PVA/CS/GQDs/Fe_2O_3 nanocomposite films were obtained using Fourier transform infrared spectrophotometer (Shimadzu, IRAffinity-1, Japan). The samples were measured in a transmission mode within the wavenumber range of 500–4000 cm^{-1}.

X-ray diffraction (XRD) pattern for the neat PVA film, PVC/CS blend, and PVA/CS/GQDs/Fe_2O_3 nanocomposites having different content of GQDs and Fe_2O_3 were investigated by employing AXS D8 (Bruker) Advanced X-ray diffractometer (Japan). The data were collected using CuKα radiation of wavelength (λ = 1.5406 Å) in the 2θ range from 10^o to 60^o having 1^o/min scanning rate and with 0.01^o step size.

The field-emission scanning electron microscopy (FESEM) for analyzing the surface morphology of PVA/CS/GQDs/Fe_2O_3 nanocomposite film with various GQDs and Fe_2O_3 loadings was analyzed by using FEI Quanta FEG 200 with 15 kV acceleration voltage.

The thermal stability of pure PVA, PVC/CS blend, and PVA/CS/GQDs/Fe_2O_3 nanocomposite film with various GQDs and Fe_2O_3 loadings was studied by using thermogravimetric analyzer (Shimadzu TGA-50), under nitrogen atmosphere. The samples were heated to 800 °C at a rate of 10 °C per minute.

The dielectric properties for pure PVA, PVC/CS blend, and PVA/CS/GQDs/Fe_2O_3 nanocomposite film having different content of GQDs and Fe_2O_3 were evaluated using PSM1735 Impedance analyzer (Newtons 4th Ltd., UK). The samples were placed in a computer-controlled furnace with a temperature range of 40 °C–650 °C and a precision of ±0.2 °C. The measurements were carried out at a temperature (40 °C–150 °C range) and in the frequency (50 Hz–20 MHz range) with the supplied voltage of 2V. The experimental impedance data were compared with fitted curves and the corresponding equivalent circuits were evaluated by using ZSim 3.20 software.

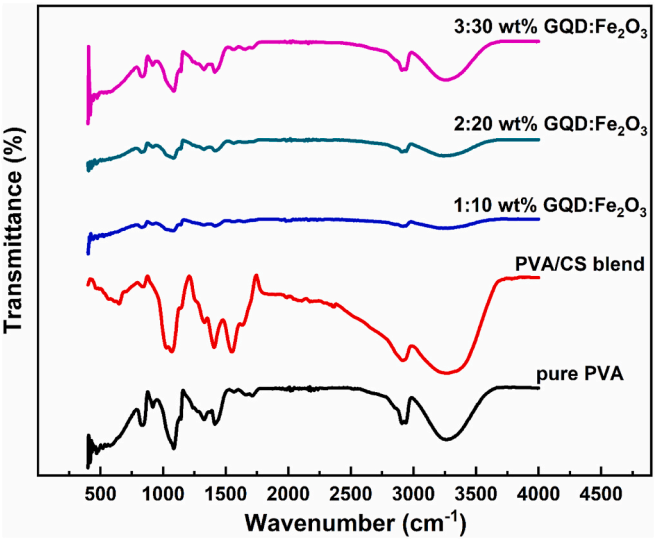

Fig. 3. FTIR spectra of (a) neat PVA, (b) PVA/CS blend, and PVA/CS/GQDs/Fe_2O_3 nanocomposites with (c) 1:10 wt%, (d) 2:20 wt%, and (e) 3:30 wt% of GQDs:Fe_2O_3 loadings.

4. Results and discussion

4.1. FTIR

The FTIR spectra of neat PVA, PVA/CS blend and PVA/CS/GQDs/Fe_2O_3 nanocomposite films illustrated in Fig. 3. In PVA (Fig. 3(a)), the strong bands detected at 3261 cm^{-1}, 1413 cm^{-1}, 1325 cm^{-1} and 1236 cm^{-1} are related to the O–H stretching vibration, CH_2 bending and C–H vibrations, respectively. The asymmetric stretching vibration of the alkyl group can be seen at 2907 cm^{-1} and 2941 cm^{-1} [44]. The vibration of the acetate group of C═O stretching appeared at 1712 cm^{-1}. Also, the C–O stretching of the acetyl group corresponding to the crystalline nature of PVA and can be seen at 1145 cm^{-1}, while the amorphous nature of PVA is observed at 1084 cm^{-1} [45,46]. After blending PVA with CS, the significant characteristic peaks of PVA with minor shifts are observed and can be seen in Fig. 3(b). For PVA/CS blend, the shift for O–H stretching vibration at 3261 cm^{-1} to 3275 cm^{-1} indicates the formation of a hydrogen bond between the PVA and CS [47]. However, the shifts at 1413 cm^{-1} to 1411 cm^{-1} and 2941 cm^{-1} to 2948 cm^{-1} indicate the interaction of the CS chain with the PVA chains. Meanwhile, peaks assigned to O═C–NHR stretching vibration of the carbonyl group and vibrations related to N–H bonding of the amino group appeared at 1641 cm^{-1} and 1558 cm^{-1}, respectively. Also, the peak that appeared at 1078 cm^{-1} corresponds to the vibrations of C–N bending of CS and C–OH stretching of PVA, while the peak at 839 cm^{-1} suggests the interaction of skeletal vibration of PVA and saccharide structure of CS. Additionally, stronger transmittance is observed for the most of bands than that of pure PVA confirming the miscibility and compatibility between PVA and CS [48]. For PVA/CS/GQDs/Fe_2O_3 nanocomposites having various loadings of GQDs and Fe_2O_3, characteristic FTIR peaks are observed to be similar to that for pure PVA and PVA/CS blend as illustrated in Fig. 3(c–e). The O–H bands and alkyl group peaks shifted to a higher wavenumber. The peaks corresponding to O═C–NHR stretching and N–H bonding are shifted to the higher wavenumber and the peaks at 1649 cm^{-1} and 1562 cm^{-1} become more intense when the nanofiller loadings increased [49,50]. Likewise, the peak consistent with vibrations of C–N bending related to CS and C–OH stretching of PVA shifted to a higher wavenumber at 1085 cm^{-1}, whereas the intensity is reduced to the minimum indicating the reduction in crystallinity of PVA [51]. The interaction peak corresponding to the skeletal vibration of PVA and saccharide structure of CS also showed a shift to a lower

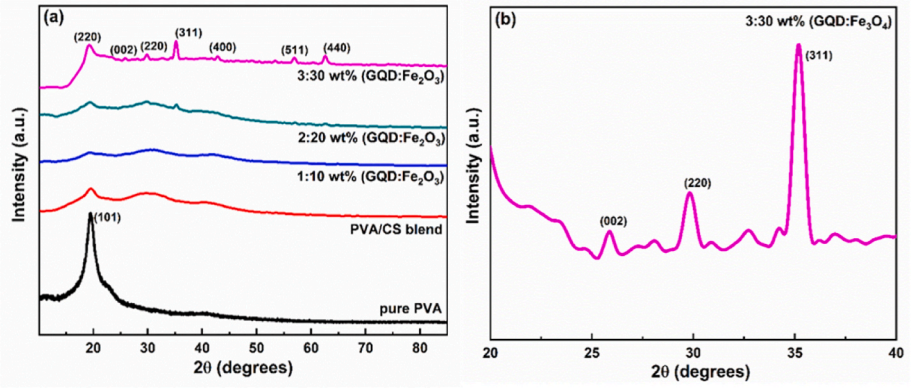

Fig. 4. (a) XRD spectra of pure PVA film, PVA/CS blend, and PVA/CS/GQDs/Fe_2O_3 nanocomposites with 1:10 wt%, 2:20 wt%, and 3:30 wt% of GQDs:Fe_2O_3 loadings (b) XRD peak of GQDs for PVA/CS/GQDs/Fe_2O_3 nanocomposite.

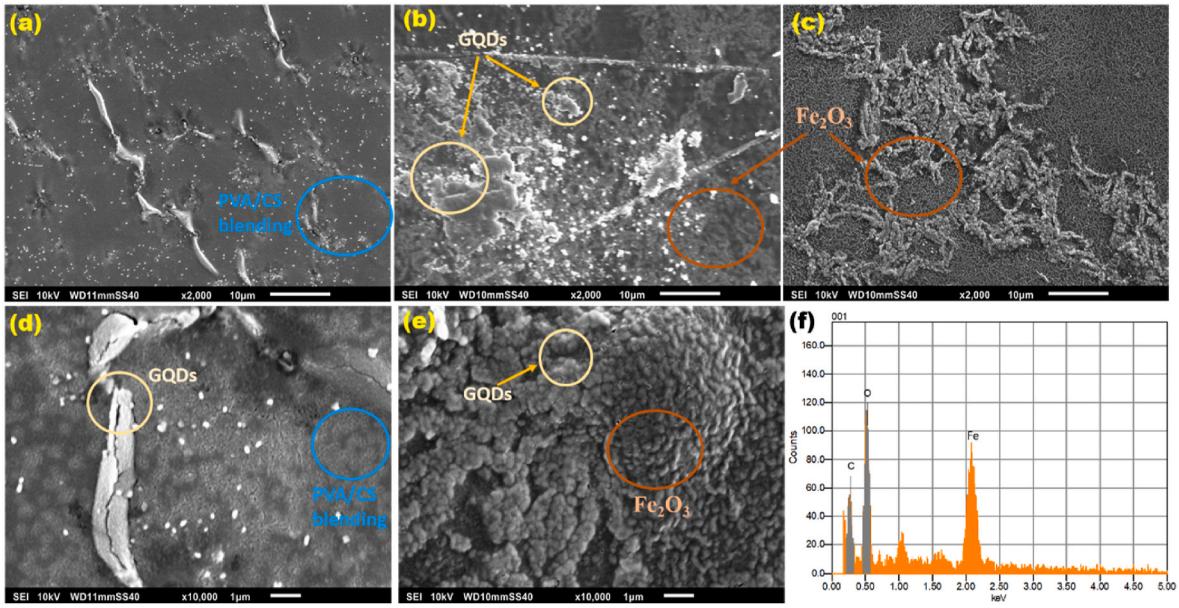

Fig. 5. SEM monographs at 10 μm resolution for (a) 1:10 wt%, (b) 2:20 wt%, and (c) 3:30 wt% of GQDs:Fe_2O_3 loadings and SEM monographs at 1 μm resolution for (d) 1:10 wt% and (e) 3:30 wt% of GQDs:Fe_2O_3 loadings, (f) EDX spectra for PVA/CS/GQDs/Fe_2O_3 nanocomposite with 3:30 wt% of GQDs:Fe_2O_3 loading.

wavenumber and reduction in intensity for lower loading of nanofillers signifying the complexation between the functional groups of nanofillers and two polymers (Fig. 3(c)). However, it is noteworthy that all the peaks and bands are less intense for lower nanofiller content and become more intense with increasing nanofillers concentration, resulting from the bond formation between the polymer blend, GQDs and Fe_2O_3 NPs [52,53]. (Fig. 3(e)). This confirms the compatibility of GQDs and Fe_2O_3 with the polymeric chains.

4.2. XRD

The XRD spectra for PVA/CS/GQDs/Fe_2O_3 nanocomposites with various content of both nanofillers along with pure PVA and polymer blend samples is illustrated in Fig. 4. The XRD pattern for neat PVA shows an intense peak at $2\theta = 19.5^\circ$, ensuring the semi-crystalline nature related to the intermolecular hydrogen bonding of PVA which is corresponding to the (101) orthorhombic lattice crystal plane [45,54]. For the PVA/CS blend, a less prominent shoulder peak arises at $2\theta = 19.8^\circ$, which belongs to the (020) crystal plane of CS in addition to the diffraction peaks of PVA [55]. Also, there are broad peaks appeared for PVA/CS blend in the $2\theta = 25^\circ$–35° region possibly due to the amorphous nature of polymers, particularly those containing CS (Fig. 4 (a)). On adding GQDs and Fe_2O_3 in the polymer blend, the diffraction peaks related to polymers become less intense and characteristic peaks related to GQDs appeared at $2\theta = 25.7^\circ$ which is quite less intense due to the small size of GQDs (Fig. 4(b)). However, the peak related to Fe_2O_3 were found at $2\theta = 30.10^\circ$, 35.45°, 43.08°, 56.90° and 62.6°, corresponding to the crystal planes (220), (311), (400), (511) and (440). The characteristic peaks obtained for the Fe_2O_3 are matching with JCPDS card no. 860550 [56,57]. Additionally, the peaks corresponding to the presence of GQDs and Fe_2O_3 are quite more intense for higher nanofiller loadings than that of the lower content of nanofillers in the PVA/CS/GQDs/Fe_2O_3. This can be due to the interaction of nanofillers with the polymer matrix [58]. Also, it indicates the structural modifications in the nanocomposite due to GQDs and Fe_2O_3. Moreover, the broad peaks related to the amorphous nature of CS decreased and almost disappeared for higher filler loading due to a decrease in CS content and increasing content of nanofillers.

4.3. SEM

The SEM monographs and EDX spectra presenting the surface

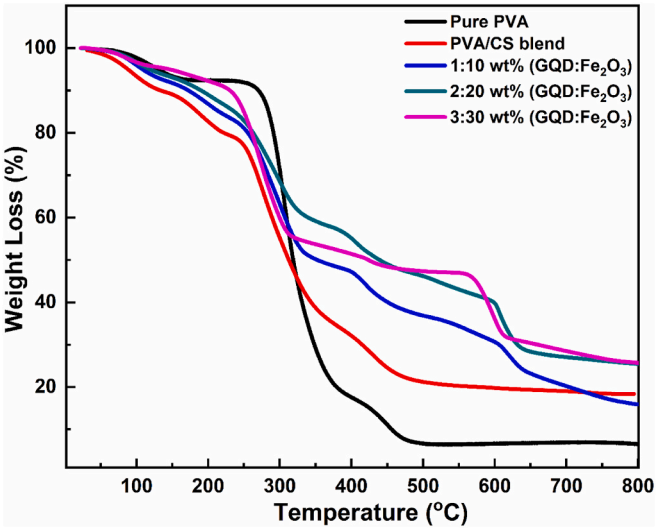

Fig. 6. TGA graph for pure PVA, PVA/CS blend, and PVA/CS/GQDs/Fe_2O_3 nanocomposites with 1:10 wt%, 2:20 wt%, and 3:30 wt% of GQDs:Fe_2O_3 loadings.

morphology of PVA/CS/GQDs/Fe_2O_3 nanocomposites with different content of GQDs and Fe_2O_3 at 10 μm and 1 μm resolution are given in Fig. 5. The nanocomposite with 1:10 wt% of GQDs:Fe_2O_3 loading represents the wrinkled structure along with white particles corresponding to the adhesion of GQDs and Fe_2O_3 (Fig. 5(a)) [59,60]. Also, the grey spots can be seen in Fig. 5(d), which indicates the homogenous blending of CS on the smooth surface of PVA [50]. In Fig. 5(b), due to the increase in the loading of nanofillers, the flakes of GQDs are more visible and aggregates of Fe_2O_3 also increased on the surface of the PVA/CS blend [61]. In the higher nanofiller loading, more discrete aggregates appeared presenting the GQDs and Fe_2O_3 adhesion (Fig. 5(c)). Additionally, there is a sphere-like morphology that can be seen in Fig. 5(e) at 1 μm resolution for the nanocomposite having 3:30 wt% of GQDs:Fe_2O_3 loadings [62,63]. In Fig. 5(f) the EDX spectra reveal the presence of elements in the PVA/CS/GQDs/Fe_2O_3 nanocomposite. The oxygen content is nearly 68 mass % present in the nanocomposite. However, the characteristic energy level for C, O and Fe is located at 0.35, 0.50 and 2.15 keV, respectively. The EDX spectra of different elements validate the presence of elements related to GQDs and Fe_2O_3 [64].

4.4. TGA

Fig. 6 represents the TGA curves demonstrating the thermal degradation behaviour of pure PVA, PVA/CS blend and PVA/CS/GQDs/Fe_2O_3 nanocomposites with different nanofiller loadings. Pure PVA follows three-step degradation in which initial degradation occurred till 240 °C having 8% weight loss indicating the evaporation of assimilated loosely bonded water molecules [65]. Further, the thermal degradation occurred in between 240 °C to 400 °C temperature range involving 75% weight loss. This step relates to the dehydration processes triggered by the structural heat degradation of the polymer [66]. The final degradation indicates the decomposition of the residue occurred beyond

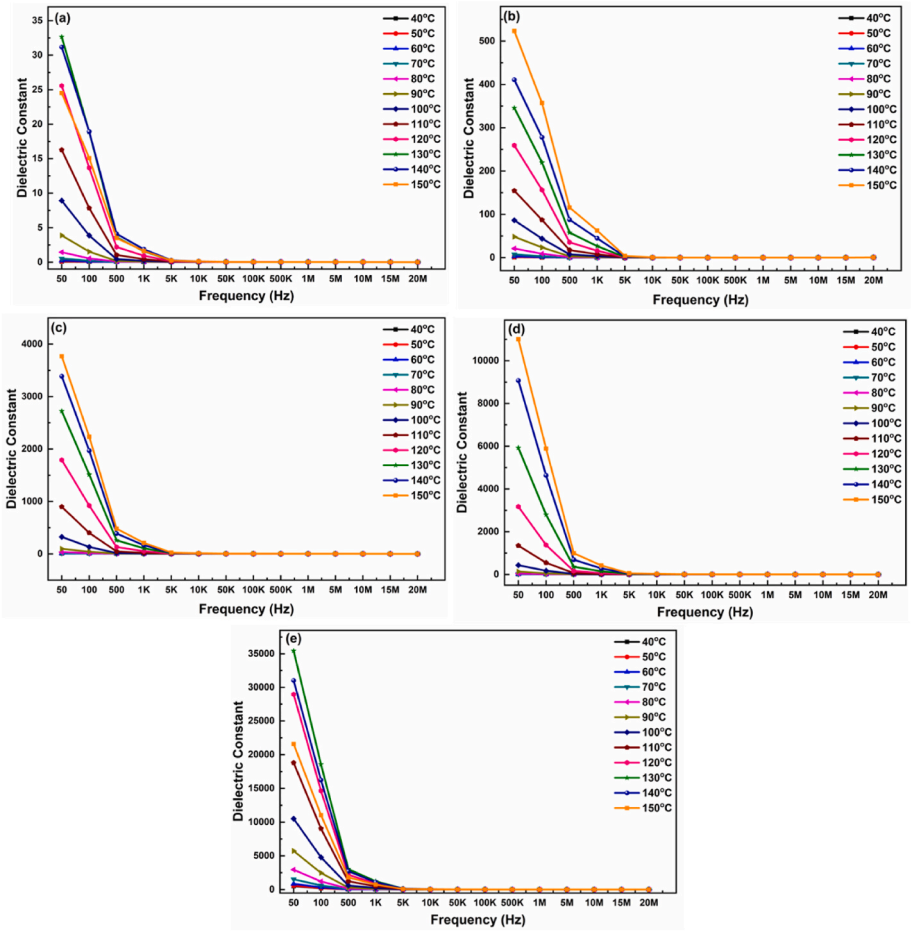

Fig. 7. Dielectric constant as a function of frequency for (a) pure PVA, (b) PVA/CS blend and PVA/CS/GQDs/Fe_2O_3 nanocomposites with (c) 1:10 wt%, (d) 2:20 wt %, and (e) 3:30 wt% of GQDs:Fe_2O_3 loadings.

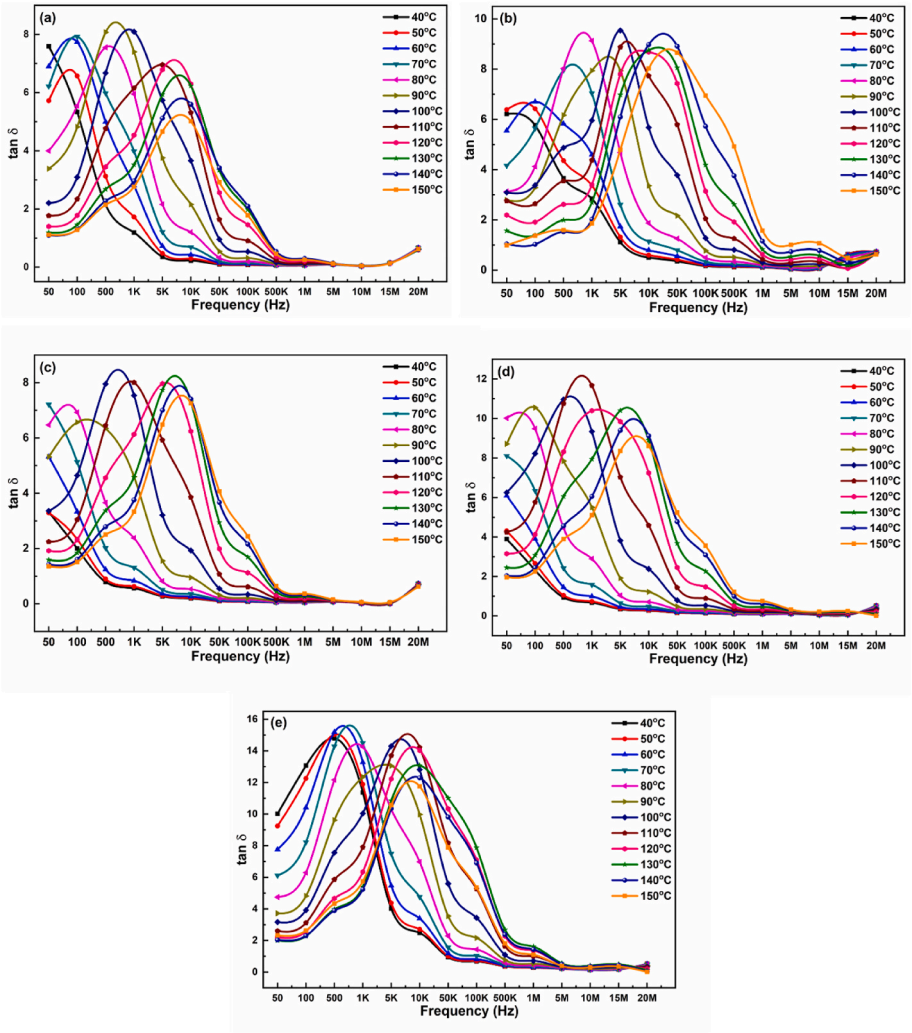

Fig. 8. Loss tangent (tan δ) as a function of frequency for (a) pure PVA, (b) PVA/CS blend and PVA/CS/GQDs/Fe_2O_3 nanocomposites with (c) 1:10 wt%, (d) 2:20 wt %, and (e) 3:30 wt% of GQDs:Fe_2O_3 loadings.

400 °C temperature with almost 11% weight loss. The thermal degradation for PVA/CS blend occurred in three different stages at 30 °C-240 °C, 240 °C-490 °C and beyond 490 °C involving 22%, 57% and 2% respectively. It begins with the moisture evaporation at the initial stage, then the side groups elimination along the breakage of PVA and CS polymer backbone chains [67]. The residue disintegration occurred at the final stage. Although, there is almost 20% residue left mainly the char residue indicating the better thermal stability of polymer blend rather than pure PVA film [68]. However, on introducing GQDs and Fe_2O_3 in the polymer blend the thermal stability was found to be improved. It can be seen in the TGA curve of PVA/CS/GQDs/Fe_2O_3 nanocomposites with 1:10 wt% of GQDs:Fe_2O_3 loadings. The initial degradation with 18% weight loss till 240 °C was due to the reduction of adsorbed water, followed by 35% weight loss between 240 °C-400 °C temperature indicating the pyrolysis of oxygen-containing functional groups of GQDs and decomposition of organic layers of Fe_2O_3 [69]. The final degradation of 15% weight loss beyond 400 °C temperature was due to the core fraction of GQDs [70]. The leftover residue was 18%, similar to PVA/CS blend film. While for the higher nanofiller loadings following the same degradation trend, the residue left is nearly 25%. It is clear from the TGA curves, that maximum thermal stability is found for the higher filler loadings involving a higher quantity of leftover residue (i.e., char residue of CS, GQDs and Fe_2O_3) than that of other samples. This improved thermal stability might have resulted from the presence of higher carbon content due to GQDs and the organic layers of Fe_2O_3 which somehow restricted the heat flow in the nanocomposite leading to the lesser thermal degradation of polymer chains [71,72]. Hence, the obtained TGA results suggest the improved thermal stability of the polymer blend by reinforcing the GQDs and Fe_2O_3 loadings in the polymer matrix.

4.5. Dielectric measurements

4.5.1. Dielectric properties as a function of frequency

The measurement of dielectric properties allows a better understanding of the interconnected nature and variation of parameters on embedding nanofillers in the polymer blend. In nanocomposites, polarization occurs in association with polymer and nanofiller interfaces due to the large volume fraction of interfaces. The dielectric parameter "complex permittivity" known as the dielectric constant of material can be calculated through

$$\varepsilon' = C.d/\varepsilon_o.A$$

where, C is the measured capacitance, d corresponds to the thickness of the sample (in m), ε_o is the permittivity of free space ($8.8549\ 10^{-12}$ F/m) and A is the surface area of the sample (in m^2).

The variation of obtained dielectric constant (ε') values on varying the frequency for pure PVA, PVA/CS blend and PVA/CS/GQDs/Fe_2O_3 nanocomposites are illustrated in Fig. 7. For pure PVA, the maximum ε'

Table 2
Dielectric constant (ε') and loss tangent (tan δ) values for PVA/CS/GQDs/Fe_2O_3 nanocomposite having different GQDs and Fe_2O_3 loadings.

PVA/CS/GQDs/Fe_2O_3 nanocomposite	Dielectric constant (ε')	Loss tangent (tan δ)
Pure PVA	32.7, 130 °C, 50 Hz	8.09, 100 °C, 1 KHz
PVA/CS blend	523.4, 150 °C, 50 Hz	9.54, 100 °C, 5 KHz
1:10 wt%, GQDs:Fe_2O_3 loading	3770.5, 150 °C, 50 Hz	8.01, 110 °C, 1 KHz
2:20 wt%, GQDs:Fe_2O_3 loading	11006.2, 150 °C, 50 Hz	11.67, 110 °C, 1 KHz
3:30 wt% GQDs:Fe_2O_3 loading	35449.1, 150 °C, 50 Hz	15.18, 60 °C, 500 Hz

value was 32.7 in 50 Hz frequency and 130 °C temperature (Fig. 7(a)). After blending PVA with CS as given in Fig. 7(b), the ε′ value increased upto 523.4 in 50 Hz frequency and 150 °C temperature. This increment resulted from the space charge polarization due to the large number of defects that establish an asymmetric distribution of charges at the interfaces of the polymer blend [73,74]. On adding GQDs and Fe_2O_3 in the PVA/CS blend, the ε′ value was increased more abruptly than the polymer blend and pure PVA samples. The ε′ was found to be 3770.5, 11006.2 and 35449.1 for 1:10 wt%, 2:20 wt% and among all maximum for higher loading i.e., 3:30 wt% of GQDs:Fe_2O_3, respectively. From Fig. 7(c–e), it can be seen that ε′ is high at low frequency (50 Hz), and decreases rapidly on increasing the frequency. At low frequencies, there is more charge accumulation at grain boundaries i.e., Maxwell-Wagner interfacial polarization [75,76], which indicates the sufficient time for dipoles to align themselves with the electric field. While at high frequency, ε′ reduces due to the disability of dipoles to align quickly with the changing electric field [76]. Moreover, the addition of GQDs and Fe_2O_3 formed the intermolecular conductive network by conformation within the chain lengths of the polymer [77]. Additionally, the ε′ value increased with the increment of nanofillers loading. Generally, the addition of ferromagnetic NPs such as Fe_2O_3, having pre-orientated electric charges results in higher ε′ values [78,79]. So, by increasing the content of Fe_2O_3 and GQDs, the value of ε′ also increased in this study where the conductive pathways are formed throughout the polymer blend [77,79].

Another parameter measured is loss tangent (tan δ) with varying frequency for pure PVA, PVA/CS blend and PVA/CS/GQDs/Fe_2O_3 nanocomposites and presented in Fig. 8. For pure PVA, the tan δ measured to be 8.09 at 1 KHz frequency and 100 °C temperature. On blending PVA with CS, the tan δ value slightly increased upto 9.54 at 5 KHz frequency and 100 °C temperature. Fig. 8(c–e) represents the variation of PVA/CS/GQDs/Fe_2O_3 nanocomposites having different nanofiller loadings, along with the change in frequency. The values of tan δ increased from 8.01 to 15.18 on adding GQDs and Fe_2O_3 in the polymer blend for lower and higher nanofiller loadings, respectively. The results revealed that the presence of GQDs and Fe_2O_3 has improved the tan δ values of the nanocomposite than that of the polymer blend. This improvement is attributed to the charge carrier increment inside the nanocomposite and the space charge polarization relaxation [77,80]. However, it can be seen that at low frequency the tan δ is lower and then increased on the further increment of frequency which is due to the dominance of the Ohmic component and later on the tan δ values drops off on higher frequencies indicating the growing nature of reactive component [81]. Also, the maximum values obtained for ε′ and tan δ for all the samples are summarized in Table 2. From these results, it can be confirmed that the presence of GQDs and Fe_2O_3 in the polymer blend has significantly improved the dielectric properties of nanocomposites owing to the compatibility of nanofillers within the polymer matrix.

4.5.2. *Dielectric properties as a function of temperature*

The ε' is observed to be increased with temperature as given in Fig. 9 (a). This increment is associated with the rise in charge carrier density as a consequence of ion aggregate disintegration [82,83]. Conversely, when the temperature rises, the viscosity of the polymer blend decreases, allowing dipoles to orient themselves more rapidly in the direction of the electric field. Furthermore, the chain segments receive enough heat energy to accelerate their rotating motion, resulting in a rise in polarization [84]. Meanwhile, as depicted in Fig. 9(b) with the rise in temperature the maximum of tan δ changed to higher frequencies,

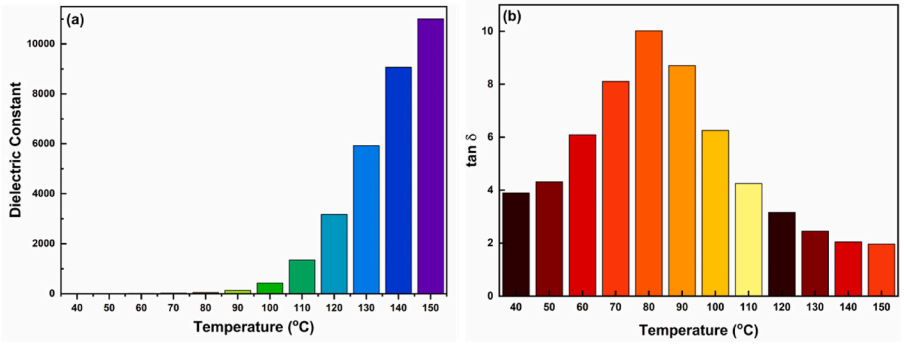

Fig. 9. (a) Dielectric constant (ε') and (b) loss tangent (tan δ) as a function of temperature for PVA/CS/GQDs/Fe_2O_3 nanocomposite having 2:20 wt% of GQDs: Fe_2O_3 loadings.

Table 3
Comparison of dielectric parameters of graphene and metal oxide based various PNCs.

Polymer nanocomposites	Nanofiller Loading (wt%)	Frequency	Dielectric constant (ε′)	Loss tangent (tan δ)	Reference
PVDF/BaTiO3/GQDs	9 wt% + 3 wt%	100 Hz	54	6	[58]
PVA/EEG	4 wt%	8–12 GHz	203	0.2	[87]
PVDF/fGNPs	6.67 wt%	100 Hz	3841	16.8	[88]
PVA/graphene	5 wt%	1 kHz	5720	0.08	[89]
PVDF/GQDs/$BaTiO_3$	3 wt% + 20 wt%	1 kHz	17249	52	[90]
PVDF/PVP/GQDs/$BaTiO_3$	3 wt% + 20 wt%	1 kHz	37993	2.3	[90]
PVA/CS/GQDs/Fe_2O_3	3 wt% + 30 wt%	50 -20 MHz	35449	15.18	This Work

Note: PVA- Poly (vinyl alcohol), PEO- Polyethylene oxide, fGNPs - functionalized Graphene nanoplates, EEG-Electrochemically exfoliated graphene, GQDs – Graphene quantum dots, CS- Chitosan, PVP- Polyvinylpyrrolidone.

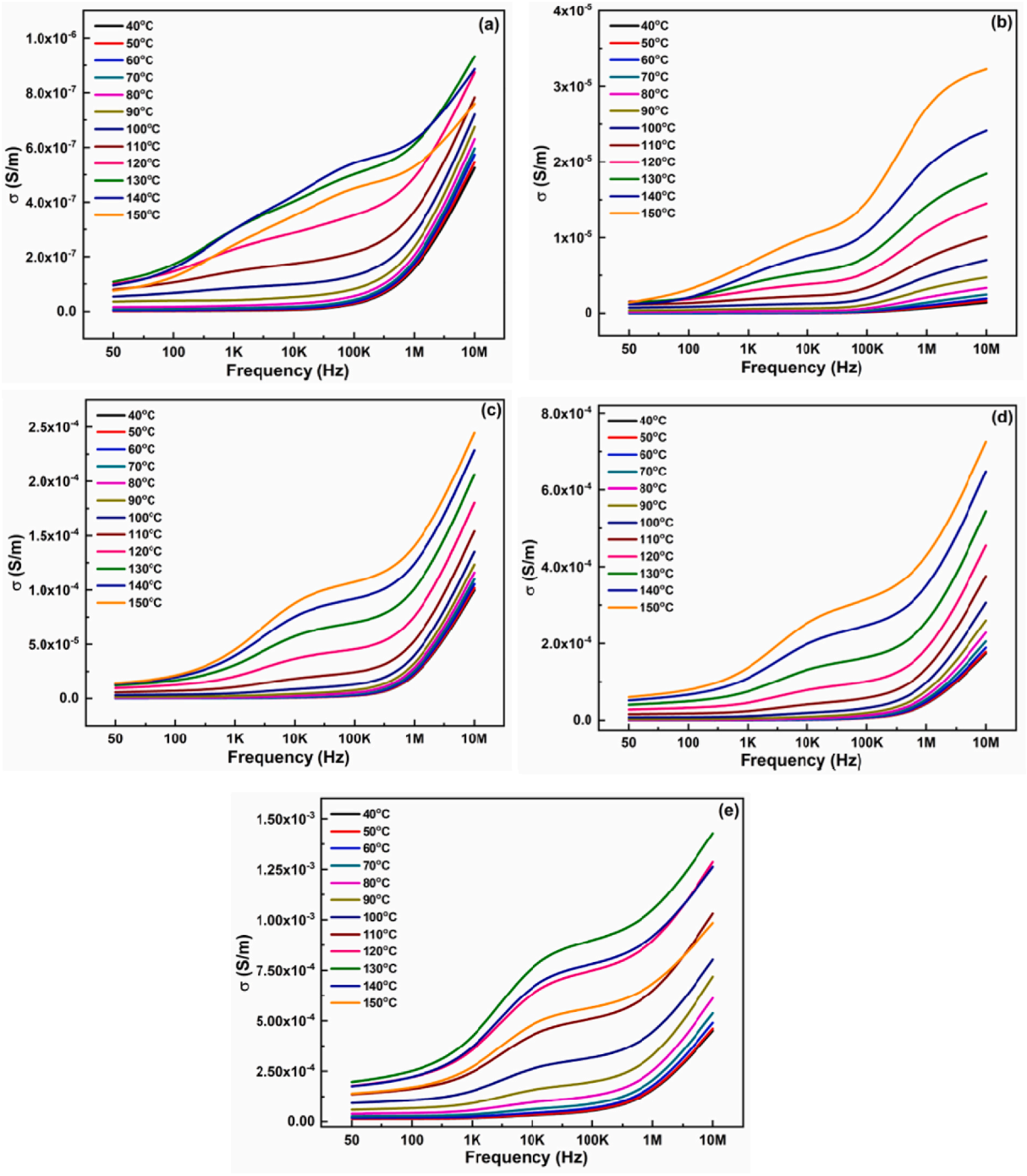

Fig. 10. AC conductivity (σ_{ac}) v/s frequency variation for (a) pure PVA, (b) PVA/CS blend and PVA/CS/GQDs/Fe_2O_3 nanocomposites with (c) 1:10 wt%, (d) 2:20 wt %, and (e) 3:30 wt% of GQDs:Fe_2O_3 loadings.

indicating that the relaxing dipoles were more dynamic [85]. Polymer chains and their connected dipoles do not move with a single relaxation time in the bulk, but rather with a variety of relaxation periods, depending on the intermolecular interactions present [86]. The relaxation time spectrum is frequently tilted toward higher frequencies. Both of these phenomena are frequent in polymer based dielectric measurements. Table 3 compares the present work with previously reported graphene and metal oxides-based various PNCs.

4.6. AC conductivity measurements

Fig. 10 represents the AC conductivity (σ_{ac}) of neat PVA, PVA/CS blend and PVA/CS/GQDs/Fe_2O_3 nanocomposites with different loadings of GQDs and Fe_2O_3 as a function of frequency at different temperatures. The σ_{ac} was found to be increased with the rise in temperature for all samples. This increment is attributed to the energy acquired by an electron at higher temperatures to move freely that leads to faster electrical conduction [52]. As evident in Fig. 10(a and b), the σ_{ac} values for pure PVA and PVA/CS blend are observed to be 9.3 x 10^{-7} (S/m) and 3.2 x 10^{-5} (S/m), respectively. Here, the formation of voids resulting from the amorphous nature of the polymer blend helps to increase conductivity with the rise in temperature [91]. The different content of GQDs and Fe_2O_3 in the polymer blend also enhanced the σ_{ac} values. For lower loading i.e., 1:10 wt% of GQDs:Fe_2O_3, the σ_{ac} measured to be 2.4 x

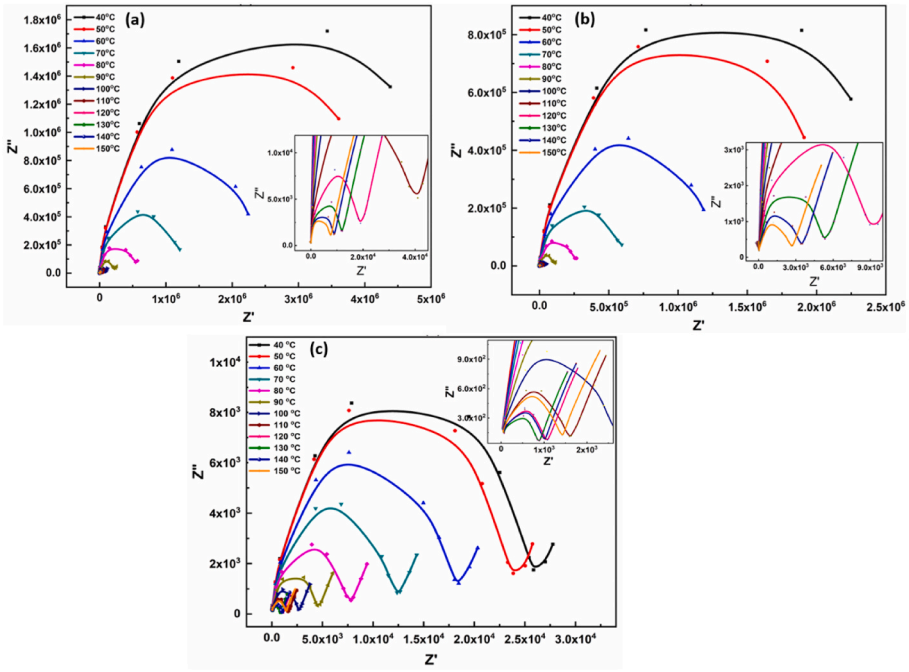

Fig. 11. Cole-Cole plot for PVA/CS/GQDs/Fe_2O_3 nanocomposite having (a) 1:10 wt%, (b) 2:20 wt%, and (c) 3:30 wt% of GQDs:Fe_2O_3 loadings.

10^{-4} (S/m) (Fig. 10(c)). The value improved on increasing the loading of nanofiller such as 7.3 x 10^{-4} (S/m) and 9.8 x 10^{-4} (S/m) for 2:20 wt% and 3:30 wt% of GQDs:Fe_2O_3 loadings, respectively at 10 MHz frequency and 150 °C temperature (Fig. 10(d and e)). Here, with the increment in the content of nanofillers, the formation of the interatomic network also increased which results in the rapid movement of free electrons and the rise in electrical conduction [92]. The frequency-dependent behaviour of σ_{ac} revealed the maximum electrical conductivity for all the nanocomposites which was attained in high-frequency regions. At low-frequency regions, because of the interfacial polarization effect, the σ_{ac} values are low as the mobile charge carriers have a limited capacity to hop from one localized state to another. On the other hand, at high-frequency regions, the mobile charge carriers are freer to move resulting from the reduction in capacitive reactance and impedance which causes the increase in the conductivity of the nanocomposites [93]. Therefore, the enhanced σ_{ac} conductivity values of nanocomposites, especially with the higher nanofiller loadings can be utilized as potential material for energy

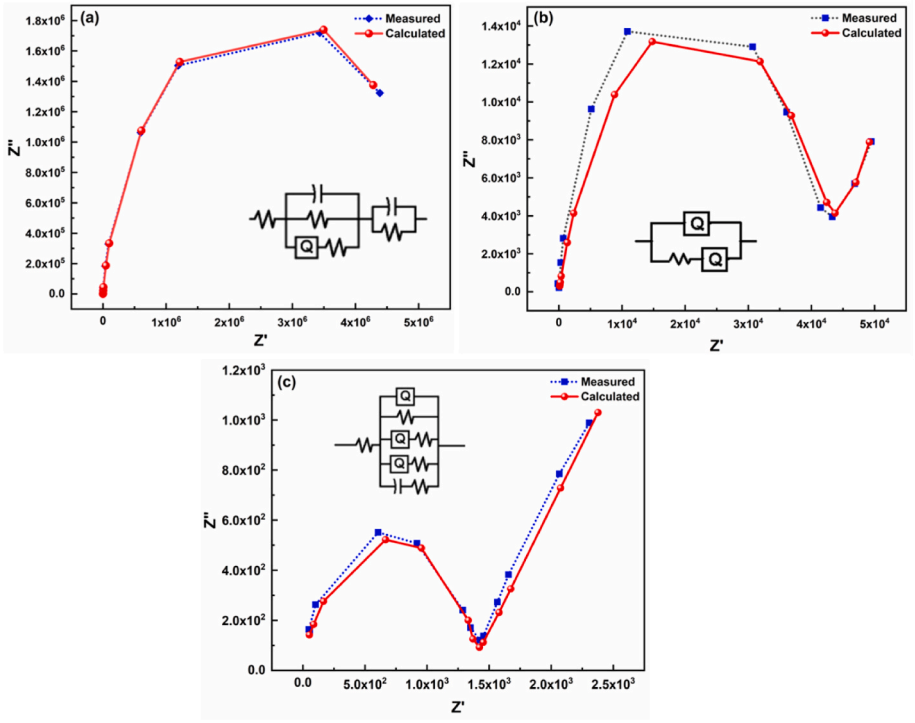

Fig. 12. Comparison of measured complex Impedance plot and fitted curve along with corresponding equivalent circuit for PVA/CS/GQDs/Fe_2O_3 nanocomposite having (a) 1:10 wt%, (b) 2:20 wt%, and (c) 3:30 wt% of GQDs:Fe_2O_3 loadings.

storage applications.

4.7. Complex impedance analysis

The impedance spectroscopy is studied for grain and grain boundary quantitative contribution in the PVA/CS/GQDs/Fe_2O_3 nanocomposite. The two components e.g., Z", the capacitive component versus Z′ the real impedance component provides the grain and grain boundary properties via successive semicircle arcs. Fig. 11 provides the cole-cole presentation of the complex impedance plots for nanocomposite having various nanofiller loadings. Typically, the Z'' versus Z′ plots discloses semicircle arcs in which the semicircle arc at a higher frequency region can be assigned to the grains whereas the semicircle arc for a lower frequency can be attributed to the grain boundary [94]. However, from the impedance plot, it can be analyzed that at low temperatures, only one semicircle arc is formed and as temperature rises, the arc is formed completely and the second semicircle spike goes on increasing corresponding to the grain boundary [95]. The higher temperature impedance curves can be seen in the insets provided in Fig. 11. Also, it is evident that on increasing the GQDs and Fe_2O_3 in the polymer blend the semicircle arcs get suppressed. This reduction in the semi-circular arcs on the addition of higher content of nanofillers may be ascribed to the formation of space charge at the polymer-nanofiller interface which might be a result of the capacitive effect and total conductivity of nanocomposites [96]. Moreover, the comparison for the measured impedance values i.e., dotted line and the fitted curves i.e., solid line, are represented in Fig. 12. The solid line confirms the best fit of the equivalent circuit in agreement with the experimental impedance data. It is also evident that the addition of different loadings of GQDs and Fe_2O_3 in the polymer blend has greatly influenced the impedance properties of the nanocomposite. Here, the first semi-circular arc is observed to be suppressed and shifted to the left side of the graphical representation as an increment in nanofiller loadings. Secondly, the spike goes on increasing with the higher content of nanofillers. So, the associated impedance was found to be decreasing with the increase in nanofiller loadings. This particularly signifies the reduction of bulk resistance and the increment of the ionic conductivity in the nanocomposites [97,98]. The corresponding equivalent circuit for the fitted curves is also provided. The equivalent circuit given as inset in the graph, consists of Q as a value of capacitance for constant phase element (CPE) (symbol ) and capacitance (C) (symbol ) in parallel combination, together with the series combination of the bulk resistance (R_b) (symbol ) [99]. Also, in real systems, the term CPE can be used in place of an ideal capacitor. The circuit shows the parallel connection of the Q, C and R_b in parallel at the high frequency and a parallel combination of C and R_b at low frequency [100]. Additionally, if the semi-circular arc exhibits a non-Debye nature, then it is expected to introduce a CPE or replace the ideal capacitor with a CPE. Also, the nanocomposite is made up of conducting nanofillers in the insulating matrix. The conductive pathways arise from the high-resistance region (polymer blend) and low-resistance region (GQDs and Fe_2O_3) [101]. The parallel combination of Q in the circuit also supports the formation of a double-layer capacitor device for energy storage applications.

5. Conclusions

The present study investigates the dielectric properties of the nanocomposites consisting of GQDs and Fe_2O_3 reinforced in PVA/CS blend via solution casting technique. The comparative evaluation of structural modifications, morphological and thermal degradation analysis has been carried out. The PVA/CS/GQDs/Fe_2O_3 nanocomposites are found to be thermally stable for higher nanofiller content. The structural modification and sphere-like morphology confirm the presence of GQDs and Fe_2O_3 interacting with the polymer blend. The frequency and temperature-dependent behaviour of various dielectric parameters are examined in the frequency range of 50 Hz to 20 MHz and at a temperature ranging from 40 °C to 150 °C. Maximum values of dielectric constant and loss tangent are measured to be 35449.1 and 15.18, respectively at 150 °C temperature and 50 Hz frequency. The higher values of the dielectric constant and corresponding low values of loss tangent suggested the potential of nanocomposites for various electrical applications. The dielectric properties and ac conductivity (σ_{ac}) of nanocomposites are greatly influenced by the addition of GQDs and Fe_2O_3. The increase in σ_{ac} immensely dependent on the increase in frequency and temperature. Also, the reduction in capacitive reactance and impedance resulted in the rise in ac conductivity upto 9.8×10^{-4} (S/m) with increasing nanofillers loadings i.e., 3:30 wt% (GQDs:Fe_2O_3). The impedance analysis provided a clear insight into grain and grain boundaries in the nanocomposites. However, the semi-circular arcs observed in the cole-cole plots are in agreement with the fitted impedance data along with the equivalent circuit. The reduction of bulk resistance and impedance on increasing the nanofiller loadings indicates the impact of GQDs and Fe_2O_3 on the properties of the nanocomposite. These significant results support the utilization of PVA/CS/GQDs/Fe_2O_3 nanocomposites as a potential candidate for energy storage applications.

CRediT authorship contribution statement

Priyanka Rani: Data curation, Formal analysis, Investigation, Writing – original draft. **Kalim Deshmukh:** Conceptualization, Formal analysis, Investigation, Resources, Data curation, Writing – review & editing, Supervision, Project administration. **Jaroslav Kadlec:** Data curation, Formal analysis, Investigation. **T.V. Krishna Karthik:** Data curation, Formal analysis, Investigation, Supervision. **S.K. Khadheer Pasha:** Formal analysis, Investigation, Resources, Supervision, Project administration.

Declaration of competing interest

The authors declare that they have no known competing financial interests or personal relationships that could have appeared to influence the work reported in this paper.

Data availability

The data that has been used is confidential.

References

[1] J. Chavhan, R. Rathod, V. Tandon, S. Umare, A. Patil, Structural and physico-chemical properties of electroactive polyamide/multi-walled carbon nanotubes nanocomposites, Surface. Interfac. (2022), 101765.
[2] X. Yang, C. Liang, T. Ma, Y. Guo, J. Kong, J. Gu, M. Chen, J. Zhu, A review on thermally conductive polymeric composites: classification, measurement, model and equations, mechanism and fabrication methods, Adv. Compos. Hybrid Mater. 1 (2018) 207–230.
[3] S. Chen, M.K. Hassanzadeh-Aghdam, R. Ansari, An analytical model for elastic modulus calculation of SiC whisker-reinforced hybrid metal matrix nanocomposite containing SiC nanoparticles, J. Alloys Compd. 767 (2018) 632–641.
[4] A.S. Das, D. Biswas, Influence of V2O5 concentration on structural and electrical transport properties of semiconducting ternary glass and glass-ceramics nanocomposite system, J. Non-Cryst. Solids 589 (2022), 121659.
[5] D. Dayananda, P.L. Reddy, K. Deshmukh, Y.R. Kumar, M.K. Kesarla, T. Kar, K. K. Sadasivuni, S.K.K. Pasha, MXene-based flexible polymer composites as high dielectric constant materials, Mxenes Their Compos (2022) 725–758.
[6] Y.R. Kumar, K. Deshmukh, T. Kovářík, S.K.K. Pasha, A systematic review on 2D materials for volatile organic compound sensing, Coord. Chem. Rev. 461 (2022), 214502.
[7] S. Panda, K. Deshmukh, S.K.K. Pasha, J. Theerthagiri, S. Manickam, M.Y. Choi, MXene based emerging materials for supercapacitor applications: recent advances, challenges, and future perspectives, Coord. Chem. Rev. 462 (2022), 214518.
[8] E.J. Bailey, K.I. Winey, Dynamics of polymer segments, polymer chains, and nanoparticles in polymer nanocomposite melts: a review, Prog. Polym. Sci. 105 (2020), 101242.

[9] S. Choudhary, R.J. Sengwa, Investigation on structural and dielectric properties of silica nanoparticles incorporated poly (ethylene oxide)/poly (vinyl pyrrolidone) blend matrix based nanocomposites, J. Inorg. Organomet. Polym. Mater. 29 (2019) 592–607.
[10] S. Choudhary, Effects of amorphous silica nanoparticles and polymer blend compositions on the structural, thermal and dielectric properties of PEO–PMMA blend based polymer nanocomposites, J. Polym. Res. 25 (2018) 1–21.
[11] R.J. Sengwa, P. Dhatarwal, S. Choudhary, A comparative study of different metal oxide nanoparticles dispersed PVDF/PEO blend matrix-based advanced multifunctional nanodielectrics for flexible electronic devices, Mater. Today Commun. 25 (2020), 101380.
[12] J.U. Jin, D.H. Lee, K.H. Nam, J. Yu, Y.K. Kim, M. Goh, S.G. Kim, H.S. Lee, B.C. Ku, N.H. You, Methylpiperidine-functionalized graphene oxide for efficient curing acceleration and gas barrier of polymer nanocomposites, Appl. Surf. Sci. 464 (2019) 509–515.
[13] F.E. Bouharras, M. Raihane, B. Ameduri, Recent progress on core-shell structured BaTiO3@ polymer/fluorinated polymers nanocomposites for high energy storage: synthesis, dielectric properties and applications, Prog. Mater. Sci. 113 (2020), 100670.
[14] Q. Song, W. Zhu, Y. Deng, M. Zhu, Q. Zhang, Synergetic optimization of thermal conductivity and breakdown strength of boron nitride/poly (vinylidene fluoride) composite film with sandwich intercalated structure for heat management in flexible electronics, Compos. Part A Appl. Sci. Manuf. 135 (2020), 105933.
[15] M.S.S.A. Saraswathi, A. Nagendran, D. Rana, Tailored polymer nanocomposite membranes based on carbon, metal oxide and silicon nanomaterials: a review, J. Mater. Chem. A. 7 (2019) 8723–8745.
[16] P. Pokharel, D. Xiao, F. Erogbogbo, O. Keles, A hierarchical approach for creating electrically conductive network structure in polyurethane nanocomposites using a hybrid of graphene nanoplatelets, carbon black and multi-walled carbon nanotubes, Compos. B Eng. 161 (2019) 169–182.
[17] S.A.G. Thangavelu, M. Mukherjee, K. Layana, C.D. Kumar, Y.R. Sulthana, R. R. Kumar, A. Ananthan, V. Muthulakshmi, A.B. Mandal, Biodegradable polyurethanes foam and foam fullerenes nanocomposite strips by one-shot moulding: physicochemical and mechanical properties, Mater. Sci. Semicond. Process. 112 (2020), 105018.
[18] J.H. Pu, X.J. Zha, M. Zhao, S. Li, R.Y. Bao, Z.Y. Liu, B.H. Xie, M.B. Yang, Z. Guo, W. Yang, 2D end-to-end carbon nanotube conductive networks in polymer nanocomposites: a conceptual design to dramatically enhance the sensitivities of strain sensors, Nanoscale 10 (2018) 2191–2198.
[19] M.S. De Luna, Y. Wang, T. Zhai, L. Verdolotti, G.G. Buonocore, M. Lavorgna, H. Xia, Nanocomposite polymeric materials with 3D graphene-based architectures: from design strategies to tailored properties and potential applications, Prog. Polym. Sci. 89 (2019) 213–249.
[20] S. Mazhar, A.A. Qarni, Y.U. Haq, Z.U. Haq, I. Murtaza, Promising PVC/MXene based flexible thin film nanocomposites with excellent dielectric, thermal and mechanical properties, Ceram. Int. 46 (2020) 12593–12605.
[21] C. Yuan, Y. Zhou, Y. Zhu, J. Liang, S. Wang, S. Peng, Y. Li, S. Cheng, M. Yang, J. Hu, Polymer/molecular semiconductor all-organic composites for high-temperature dielectric energy storage, Nat. Commun. 11 (2020) 1–8.
[22] H. Hosseinzadeh, S. Ramin, Effective removal of copper from aqueous solutions by modified magnetic chitosan/graphene oxide nanocomposites, Int. J. Biol. Macromol. 113 (2018) 859–868.
[23] N. Mohd Nurazzi, M.R.M. Asyraf, A. Khalina, N. Abdullah, F.A. Sabaruddin, S. H. Kamarudin, S. Ahmad, A.M. Mahat, C.L. Lee, H.A. Aisyah, Fabrication, functionalization, and application of carbon nanotube-reinforced polymer composite: an overview, Polymers (Basel) 13 (2021) 1047.
[24] A. Kausar, A review of high performance polymer nanocomposites for packaging applications in electronics and food industries, J. Plastic Film Sheeting 36 (2020) 94–112.
[25] L. Li, J. Cheng, Y. Cheng, T. Han, Y. Liu, Y. Zhou, G. Zhao, Y. Zhao, C. Xiong, L. Dong, Significant improvements in dielectric constant and energy density of ferroelectric polymer nanocomposites enabled by ultralow contents of nanofillers, Adv. Mater. 33 (2021), 2102392.
[26] P.L. Reddy, K. Deshmukh, T. Kovářík, N.A. Nambiraj, K.P. Shaik, Green chemistry mediated synthesis of cadmium sulphide/polyvinyl alcohol nanocomposites: assessment of microstructural, thermal, and dielectric properties, Polym. Compos. 41 (2020) 2054–2067.
[27] T. Remiš, P. Bělský, T. Kovářík, J. Kadlec, M. Ghafouri Azar, R. Medlín, V. Vavruňková, K. Deshmukh, K.K. Sadasivuni, Study on structure, thermal behavior, and viscoelastic properties of nanodiamond-reinforced poly (vinyl alcohol) nanocomposites, Polymers (Basel) 13 (2021) 1426.
[28] L. Gautam, S.G. Warkar, S.I. Ahmad, R. Kant, M. Jain, A review on carboxylic acid cross-linked polyvinyl alcohol: properties and applications, Polym. Eng. Sci. 62 (2022) 225–246.
[29] S. Roy, H.C. Kim, L. Zhai, J. Kim, Preparation and characterization of synthetic melanin-like nanoparticles reinforced chitosan nanocomposite films, Carbohydr. Polym. 231 (2020), 115729.
[30] A. Solikhin, Y.S. Hadi, M.Y. Massijaya, S. Nikmatin, S. Suzuki, Y. Kojima, H. Kobori, Properties of poly (vinyl alcohol)/chitosan nanocomposite films reinforced with oil palm empty fruit bunch amorphous lignocellulose nanofibers, J. Polym. Environ. 26 (2018) 3316–3333.
[31] S. Shekhar, A. Sarkar, B. Sharma, P. Jain, Electrochemical evaluation of functionalized graphene oxide filled PVA-chitosan biohybrid for supercapacitor applications, J. Appl. Polym. Sci. 137 (2020), 48610.
[32] L.D. Nguyen, T.C.D. Doan, T.M. Huynh, V.N.P. Nguyen, H.H. Dinh, D.M.T. Dang, C.M. Dang, An electrochemical sensor based on polyvinyl alcohol/chitosan-thermally reduced graphene composite modified glassy carbon electrode for sensitive voltammetric detection of lead, Sens. Actuators, B 345 (2021), 130443.
[33] T. Fan, L. Jian, C. Liu, I. Murtaza, R. Abid, A. Shuja, Y. Liu, Y. Min, Controlled synthesis of the state-of-the-art quasi one-dimensional graphene nanostructure for high performance supercapacitor, Synth. Met. 289 (2022), 117131.
[34] Y. Xu, H. Cao, Y. Xue, B. Li, W. Cai, Liquid-phase exfoliation of graphene: an overview on exfoliation media, techniques, and challenges, Nanomaterials 8 (2018) 942.
[35] Z. Zeng, S. Chen, T.T.Y. Tan, F.-X. Xiao, Graphene quantum dots (GQDs) and its derivatives for multifarious photocatalysis and photoelectrocatalysis, Catal. Today 315 (2018) 171–183.
[36] S.N.M. Shareef, K. Chidambaram, S.K.K. Pasha, Structure, morphology and dielectric properties of hexagonal boron nitride nanoparticles reinforced biopolymer nanocomposites, Polym. Technol. Mater. 58 (2019) 1210–1225.
[37] N.A.H. Al-Aaraji, A. Hashim, A. Hadi, H.M. Abduljalil, Effect of silicon Carbide nanoparticles addition on structural and dielectric characteristics of PVA/CuO nanostructures for electronics devices, Silicon 14 (2022) 4699–4705.
[38] V. Siva, D. Vanitha, A. Murugan, A. Shameem, S.A. Bahadur, Studies on structural and dielectric behaviour of PVA/PVP/SnO nanocomposites, Compos. Commun. 23 (2021), 100597.
[39] A. Badawi, S.S. Alharthi, Reinforcing the electrical and mechanical properties of the reduced graphene oxide/PVA blend using Fe2O3 nanoparticles for flexible electronic devices, J. Inorg. Organomet. Polym. Mater. (2022) 1–10.
[40] Y. Ul-Haq, I. Murtaza, S. Mazhar, R. Ullah, M. Iqbal, A.A. Qarni, S. Amin, Dielectric, thermal and mechanical properties of hybrid PMMA/RGO/Fe2O3 nanocomposites fabricated by in-situ polymerization, Ceram. Int. 46 (2020) 5828–5840.
[41] K.D. Salman, Synthesis and characterization unsaturated polyester resin nanocomposites reinforced by Fe2O3+ Ni nanoparticles: influence on mechanical and magnetic properties, Int. J. Eng. 35 (2022) 21–28.
[42] A. Deb, A. Debnath, K. Bhowmik, S. Rudra Paul, B. Saha, Application of polyaniline impregnated mixed phase Fe2O3, MnFe2O4 and ZrO2 nanocomposite for rapid abatement of binary dyes from aqua matrix: response surface optimisation, Int. J. Environ. Anal. Chem. (2021) 1–19.
[43] Y. Uysal, B. Mut, Biogas and methane production efficiency of sewage sludge supplemented with conductive materials, Int. J. Glob. Warming 20 (2020) 353–373.
[44] A. Sharif, M. Mustaqeem, T.A. Saleh, A. ur Rehman, M. Ahmad, M.F. Warsi, Synthesis, structural and dielectric properties of Mg/Zn ferrites-PVA nanocomposites, Mater. Sci. Eng. B. 280 (2022), 115689.
[45] G.J. Thangamani, K. Deshmukh, N.A. Nambiraj, S.K.K. Pasha, Chemiresistive gas sensors based on vanadium pentoxide reinforced polyvinyl alcohol/polypyrrole blend nanocomposites for room temperature LPG sensing, Synth. Met. 273 (2021), 116687.
[46] E. Olewnik-Kruszkowska, M. Gierszewska, E. Jakubowska, I. Tarach, V. Sedlarik, M. Pummerova, Antibacterial films based on PVA and PVA–chitosan modified with poly (hexamethylene guanidine), Polymers (Basel) 11 (2019) 2093.
[47] A. Farazin, M. Mohammadimehr, A.H. Ghasemi, H. Naeimi, Design, preparation, and characterization of CS/PVA/SA hydrogels modified with mesoporous Ag 2 O/SiO 2 and curcumin nanoparticles for green, biocompatible, and antibacterial biopolymer film, RSC Adv. 11 (2021) 32775–32791.
[48] X. Feng, X. Hou, C. Cui, S. Sun, S. Sadik, S. Wu, F. Zhou, Mechanical and antibacterial properties of tannic acid-encapsulated carboxymethyl chitosan/polyvinyl alcohol hydrogels, Eng. Regen. 2 (2021) 57–62.
[49] V. Soltaninejad, A. Maleki, A green, and eco-friendly bionanocomposite film (poly (vinyl alcohol)/TiO2/chitosan/chlorophyll) by photocatalytic ability, and antibacterial activity under visible-light irradiation, J. Photochem. Photobiol. Chem. 404 (2021), 112906.
[50] H. Ali, T.M. Tiama, A.M. Ismail, New and efficient NiO/chitosan/polyvinyl alcohol nanocomposites as antibacterial and dye adsorptive films, Int. J. Biol. Macromol. 186 (2021) 278–288.
[51] N.M. Sadiq, S.B. Aziz, M.F.Z. Kadir, Development of flexible plasticized ion conducting polymer blend electrolytes based on polyvinyl alcohol (PVA): chitosan (CS) with high ion transport parameters close to gel based electrolytes, Gels 8 (2022) 153.
[52] D. Arthisree, W. Madhuri, N. Saravanan, B. Dinesh, S. Saikrithika, A.S. Kumar, A ternary polymer nanocomposite film composed of green-synthesized graphene quantum dots, polyaniline, polyvinyl butyral and poly (3, 4-ethylenedioxythiophene) polystyrene sulfonate for supercapacitor application, J. Energy Storage 35 (2021), 102333.
[53] P.K. Gupta, S. Palanisamy, T. Gopal, R. Rajamani, S. Pandit, S. Sinha, V. K. Thakur, Synthesis and characterization of novel Fe3O4/PVA/eggshell hybrid nanocomposite for photodegradation and antibacterial activity, J. Compos. Sci. 5 (2021) 267.
[54] J. Ahmad, K. Deshmukh, M.B. Hägg, Influence of TiO2 on the chemical, mechanical, and gas separation properties of polyvinyl alcohol-titanium dioxide (PVA-TiO2) nanocomposite membranes, Int. J. Polym. Anal. Char. 18 (2013) 287–296.
[55] S.K.K. Pasha, K. Deshmukh, M.B. Ahamed, K. Chidambaram, M.K. Mohanapriya, N.A.N. Raj, Investigation of microstructure, morphology, mechanical, and dielectric properties of PVA/PbO nanocomposites, Adv. Polym. Technol. 36 (2017) 352–361, https://doi.org/10.1002/adv.21616.
[56] K. Raja, M.M. Jaculine, M. Jose, S. Verma, A.A.M. Prince, K. Ilangovan, K. Sethusankar, S.J. Das, Sol–gel synthesis and characterization of α-Fe2O3 nanoparticles, Superlattice. Microst. 86 (2015) 306–312.

[57] D.P. Joshi, G. Pant, N. Arora, S. Nainwal, Effect of solvents on morphology, magnetic and dielectric properties of (α-Fe2O3@ SiO2) core-shell nanoparticles, Heliyon 3 (2017), e00253.
[58] Y.R. Kumar, S.K.K. Pasha, Synergistic effect of barium titanate nanoparticles and graphene quantum dots on the dielectric properties and conductivity of poly (vinylidenefluoride-co-hexafluoroethylene) films, Environ. Res. 204 (2022), 112297.
[59] S. Javanbakht, N. Nazari, R. Rakhshaei, H. Namazi, Cu-crosslinked carboxymethylcellulose/naproxen/graphene quantum dot nanocomposite hydrogel beads for naproxen oral delivery, Carbohydr. Polym. 195 (2018) 453–459.
[60] L.P. Lingamdinne, K.R. Vemula, Y.-Y. Chang, J.-K. Yang, R.R. Karri, J.R. Koduru, Process optimization and modeling of lead removal using iron oxide nanocomposites generated from bio-waste mass, Chemosphere 243 (2020), 125257.
[61] M. Aslam, Z.A. Raza, A. Siddique, Fabrication and chemo-physical characterization of CuO/chitosan nanocomposite-mediated tricomponent PVA films, Polym. Bull. 78 (2021) 1955–1965.
[62] S.M. Siddeeg, M.A. Tahoon, W. Mnif, F. Ben Rebah, Iron oxide/chitosan magnetic nanocomposite immobilized manganese peroxidase for decolorization of textile wastewater, Processes 8 (2019) 5.
[63] M. Dinari, M.M. Momeni, M. Goudarzirad, Dye-sensitized solar cells based on nanocomposite of polyaniline/graphene quantum dots, J. Mater. Sci. 51 (2016) 2964–2971.
[64] S.S.J. Aravind, V. Eswaraiah, S. Ramaprabhu, Facile and simultaneous production of metal/metal oxide dispersed graphene nano composites by solar exfoliation, J. Mater. Chem. 21 (2011) 17094–17097.
[65] T.A. Taha, M.A.A. Alzara, Synthesis, thermal and dielectric performance of PVA-SrTiO3 polymer nanocomposites, J. Mol. Struct. 1238 (2021), 130401.
[66] S. NoormohammadShareef, K. Chidambaram, Influence of hexagonal boron nitride and BaTiO3 as hybrid fillers on the structural, morphological and dielectric behavior of polyvinyl alcohol nanocomposites, Mater. Today Proc. 9 (2019) 142–155.
[67] M.M. Atta, E.O. Taha, A.M. Abdelreheem, Nitrogen plasma effect on the structural, thermal, and dynamic mechanical properties of PVA/starch/graphene oxide nanocomposite, Appl. Phys. A 127 (2021) 1–10.
[68] A. Naeimi, M. Payandeh, A.R. Ghara, F.E. Ghadi, In vivo evaluation of the wound healing properties of bio-nanofiber chitosan/polyvinyl alcohol incorporating honey and Nepeta dschuparensis, Carbohydr. Polym. 240 (2020), 116315.
[69] L. Guo, H. Chen, N. He, Y. Deng, Effects of surface modifications on the physicochemical properties of iron oxide nanoparticles and their performance as anticancer drug carriers, Chin. Chem. Lett. 29 (2018) 1829–1833.
[70] A. Porfarzollah, R. Mohammad-Rezaei, M. Bagheri, Ionic liquid-functionalized graphene quantum dots as an efficient quasi-solid-state electrolyte for dye-sensitized solar cells, J. Mater. Sci. Mater. Electron. 31 (2020) 2288–2297.
[71] B.V.M. Rodrigues, T.S. Cabral, L.F. Sgobbi, J.A.M. Delezuk, R.S. Pessoa, E. R. Triboni, T.B.F. de Moraes, A.O. Lobo, A simple and green method for the production of nanostructured materials from poly (vinyl alcohol)/graphene quantum dots, Mater. Chem. Phys. 219 (2018) 242–250.
[72] R. Ahmad, A. Mirza, Facile one pot green synthesis of Chitosan-Iron oxide (CS-Fe2O3) nanocomposite: removal of Pb (II) and Cd (II) from synthetic and industrial wastewater, J. Clean. Prod. 186 (2018) 342–352.
[73] J. Sun, H. Choi, S. Cha, D. Ahn, M. Choi, S. Park, Y. Cho, J. Lee, T. Park, J. Park, Highly enhanced triboelectric performance from increased dielectric constant induced by ionic and interfacial polarization for chitosan based multi-modal sensing system, Adv. Funct. Mater. 32 (2022), 2109139.
[74] M.K. Hassan, A. Abukmail, A.J. Hassiba, K.A. Mauritz, A.A. Elzatahry, PVA/chitosan/silver nanoparticles electrospun nanocomposites: molecular relaxations investigated by modern broadband dielectric spectroscopy, Nanomaterials 8 (2018) 888.
[75] A.K. Chaturvedi, A. Pappu, M.K. Gupta, Unraveling the role of agro waste-derived graphene quantum dots on dielectric and mechanical property of the fly ash based polymer nanocomposite, J. Alloys Compd. 903 (2022), 163953.
[76] A.K. Chaturvedi, A. Pappu, A.K. Srivastava, M.K. Gupta, Synthesis dielectric and mechanical properties of paddy straw derived graphene quantum dots-stone waste nanocomposite, Mater. Lett. 301 (2021), 130323.
[77] Y.R. Kumar, K. Deshmukh, M.M.N. Ali, G. Abhijay, W.A. Al-Onazi, A.M. Al-Mohaimeed, S.K.K. Pasha, Structure, morphology and modelling studies of polyvinylalcohol nanocomposites reinforced with nickel oxide nanoparticles and graphene quantum dots, Environ. Res. 203 (2022), 111842.
[78] L.M. Gradinaru, M. Barbalata Mandru, M. Drobota, M. Aflori, M. Butnaru, M. Spiridon, F. Doroftei, M. Aradoaei, R.C. Ciobanu, S. Vlad, Composite materials based on iron oxide nanoparticles and polyurethane for improving the quality of MRI, Polymers (Basel) 13 (2021) 4316.
[79] Q. Jebur, A. Hashim, M. Habeeb, Fabrication, structural and optical properties for (polyvinyl alcohol–polyethylene oxide–iron oxide) nanocomposites, Egypt, J. Chem. 63 (2020) 611–623.
[80] Q. Hu, Y. Fang, Z. Du, Z. Guo, Z. Liu, Y. Huang, J. Lin, C. Tang, Controllable synthesis and enhanced microwave absorption properties of novel lightweight graphene quantum dots/hexagonal boron nitride composites, Carbon N. Y. 182 (2021) 134–143.
[81] A. Arya, A.L. Sharma, Temperature and salt-dependent dielectric properties of blend solid polymer electrolyte complexed with LiBOB, Macromol. Res. 27 (2019) 334–345.
[82] Q. Li, L. Chen, M.R. Gadinski, S. Zhang, G. Zhang, H.U. Li, E. Iagodkine, A. Haque, L.-Q. Chen, T.N. Jackson, Flexible high-temperature dielectric materials from polymer nanocomposites, Nature 523 (2015) 576–579.
[83] Y.A. Hassan, H. Hu, Current status of polymer nanocomposite dielectrics for high-temperature applications, Compos. Part A Appl. Sci. Manuf. 138 (2020), 106064.
[84] R.M. Ahmed, R.M.M. Morsi, Polymer nanocomposite dielectric and electrical properties with quantum dots nanofiller, Mod. Phys. Lett. B 31 (2017), 1750278.
[85] M. Vandana, H. Vijeth, S.P. Ashokkumar, H. Devendrappa, Graphene quantum dots doped conducting polymer nanocomposite for high performance supercapacitor application, Int. J. Nanotechnol. 18 (2021) 494–504.
[86] S. Sinha, S.K. Chatterjee, J. Ghosh, A.K. Meikap, Dielectric relaxation and ac conductivity behaviour of polyvinyl alcohol–HgSe quantum dot hybrid films, J. Phys. D Appl. Phys. 47 (2014), 275301.
[87] A. Shayesteh Zeraati, F. Sharif, E. Aliabadian, E.P.L. Roberts, U. Sundararaj, Co-doped electrochemically exfoliated graphene/polymer nanocomposites with high dielectric constant and low dielectric loss for flexible dielectrics and charge storage, ACS Appl. Nano Mater. 3 (2020) 4512–4521.
[88] U.O. Uyor, A.P.I. Popoola, O.M. Popoola, V.S. Aigbodion, Mechanically insulated graphene/polymer nanocomposites with improved dielectric performance and energy storage capacity, Polym. Sci. Ser. A. 60 (2018) 875–885.
[89] Z. Wang, N.M. Han, Y. Wu, X. Liu, X. Shen, Q. Zheng, J.-K. Kim, Ultrahigh dielectric constant and low loss of highly-aligned graphene aerogel/poly (vinyl alcohol) composites with insulating barriers, Carbon N. Y. 123 (2017) 385–394.
[90] N.V. Lakshmi, P. Tambe, N.K. Sahu, Giant permittivity of three phase polymer nanocomposites obtained by modifying hybrid nanofillers with polyvinylpyrrolidone, Compos. Interfac. 25 (2018) 47–67.
[91] E.M. Abdelrazek, A.M. Abdelghany, A.E. Tarabiah, H.M. Zidan, AC conductivity and dielectric characteristics of PVA/PVP nanocomposite filled with MWCNTs, J. Mater. Sci. Mater. Electron. 30 (2019) 15521–15533.
[92] M.J. Tommalieh, H.A. Ibrahium, N.S. Awwad, A.A. Menazea, Gold nanoparticles doped polyvinyl alcohol/chitosan blend via laser ablation for electrical conductivity enhancement, J. Mol. Struct. 1221 (2020), 128814.
[93] P.R. Kharangarh, N.M. Ravindra, R. Rawal, A. Singh, V. Gupta, Graphene quantum dots decorated on spinel nickel cobaltite nanocomposites for boosting supercapacitor electrode material performance, J. Alloys Compd. 876 (2021), 159990.
[94] K.M. Batoo, S. Kumar, C.G. Lee, Study of dielectric and ac impedance properties of Ti doped Mn ferrites, Curr. Appl. Phys. 9 (2009) 1397–1406.
[95] K. Deshmukh, M.B. Ahamed, A.R. Polu, K.K. Sadasivuni, S.K. Pasha, D. Ponnamma, M.A.-A. AlMaadeed, R.R. Deshmukh, K. Chidambaram, Impedance spectroscopy, ionic conductivity and dielectric studies of new Li+ ion conducting polymer blend electrolytes based on biodegradable polymers for solid state battery applications, J. Mater. Sci. Mater. Electron. 27 (2016) 11410–11424.
[96] K.S. Hemalatha, G. Sriprakash, M.V.N. Ambika Prasad, R. Damle, K. Rukmani, Temperature dependent dielectric and conductivity studies of polyvinyl alcohol-ZnO nanocomposite films by impedance spectroscopy, J. Appl. Phys. 118 (2015), 154103.
[97] A. Arya, A.L. Sharma, Effect of salt concentration on dielectric properties of Li-ion conducting blend polymer electrolytes, J. Mater. Sci. Mater. Electron. 29 (2018) 17903–17920.
[98] M. Ates, M.A. Serin, I. Ekmen, Y.N. Ertas, Supercapacitor behaviors of polyaniline/CuO, polypyrrole/CuO and PEDOT/CuO nanocomposites, Polym. Bull. 72 (2015) 2573–2589.
[99] R. Barik, B.K. Jena, A. Dash, M. Mohapatra, In situ synthesis of flowery-shaped α-FeOOH/Fe 2 O 3 nanoparticles and their phase dependent supercapacitive behaviour, RSC Adv. 4 (2014) 18827–18834.
[100] M.M. Nofal, S.B. Aziz, M.A. Brza, S.N. Abdullah, E.M.A. Dannoun, J.M. Hadi, A. R. Murad, S.I. Al-Saeedi, M.F.Z. Kadir, Studies of circuit design, structural, relaxation and potential stability of polymer blend electrolyte membranes based on PVA: MC impregnated with NH4I salt, Membranes (Basel) 12 (2022) 284.
[101] K.S. Hemalatha, G. Sriprakash, M.V.N. Ambika Prasad, R. Damle, K. Rukmani, Temperature dependent dielectric and conductivity studies of polyvinyl alcohol-ZnO nanocomposite films by impedance spectroscopy, J. Appl. Phys. 118 (2015), 154103.